Heliyon 10 (2024) e26354

Contents lists available at ScienceDirect

Heliyon

journal homepage: www.cell.com/heliyon

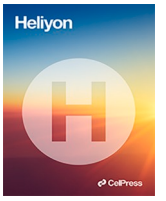

Research article

On the generality of the finite element modeling physical fields in biological systems by the multiscale smeared concept (Kojic transport model)

Milos Kojic [a,b,c,*], Miljan Milosevic [b,d,e], Vladimir Simic [b,d], Bogdan Milicevic [b,f], Rossana Terracciano [a,g], Carly S. Filgueira [a,h]

[a] Houston Methodist Research Institute, The Department of Nanomedicine, 6670 Bertner Ave., R7 117, Houston, TX, 77030, USA
[b] Bioengineering Research and Development Center BioIRC Kragujevac, Prvoslava Stojanovica 6, 3400, Kragujevac, Serbia
[c] Serbian Academy of Sciences and Arts, Knez Mihailova 35, 11000, Belgrade, Serbia
[d] Institute of Information Technologies, University of Kragujevac, Department of Technical- Technological Sciences, Jovana Cvijica bb, 34000, Kragujevac, Serbia
[e] Belgrade Metropolitan University, Tadeusa Koscuska 63, 11000, Belgrade, Serbia
[f] Faculty of Engineering, University of Kragujevac, Kragujevac, 34000, Serbia
[g] Department of Electronics and Telecommunications, Politecnico di Torino, Torino, Italy
[h] Department of Cardiovascular Surgery, Houston Methodist Research Institute, Houston, TX, 77030, USA

ARTICLE INFO

Keywords:
Convective-diffusive transport
Kojic transport model
Multiscale-multiphysics models
Composite smeared finite element
Lung parenchyma

ABSTRACT

The biomechanical and biochemical processes in the biological systems of living organisms are extremely complex. Advances in understanding these processes are mainly achieved by laboratory and clinical investigations, but in recent decades they are supported by computational modeling. Besides enormous efforts and achievements in this modeling, there still is a need for new methods that can be used in everyday research and medical practice. In this report, we give a view of the generality of the finite element methodology introduced by the first author and supported by his collaborators. It is based on the multiscale smeared physical fields, termed as Kojic Transport Model (KTM), published in several journal papers and summarized in a recent book (Kojic et al., 2022) [1]. We review relevant literature to demonstrate the distinctions and advantages of our methodology and indicate possible further applications. We refer to our published results by a selection of a few examples which include modeling of partitioning, blood flow, molecular transport within the pancreas, multiscale-multiphysics model of coupling electrical field and ion concentration, and a model of convective-diffusive transport within the lung parenchyma. Two new examples include a model of convective-diffusive transport within a growing tumor, and drug release from nanofibers with fiber degradation.

1. Introduction

Biological systems in living organisms are generally more complex when compared to others in nature. Physico-chemical laws are

* Corresponding author. Houston Methodist Research Institute, The Department of Nanomedicine, 6670 Bertner Ave., R7 117, Houston, TX, 77030, USA.
E-mail address: mkojic42@gmail.com (M. Kojic).

https://doi.org/10.1016/j.heliyon.2024.e26354
Received 17 July 2023; Received in revised form 9 February 2024; Accepted 12 February 2024
Available online 23 February 2024

equally applicable to mechanical systems within the living as in the general environment. But, there are specific processes in the living systems, such as, for example, a transformation of the biochemical into mechanical energy with temporarily succeeding events occurring in orders of magnitude different time and length scales. Or, the heart represents an electro-mechanical system that involves the generation of electrical impulses with strictly determined waves, transferred through a neural fiber network to reach muscle cell membranes, and causing a change of the membrane potential; further, change of calcium concentration within cells ultimately produces conformational changes of molecules of the sarcomere to produce mechanical force. The internal mechanical force represents the heart muscle's action to pump the blood from the heart to the arterial network.

There is a huge number of scientific papers, books, and reports on computational methods applied to model mechanics and physical fields in biomedical engineering. Before the computer era, starting in the nineteen-fifties, the methods were based, as in other fields of science and engineering, on analytically derived expressions with various functional forms such as special functions, integral transforms, finite and infinite series, etc. The development of computational methods, with the use of computers and specific software, revolutionalized mathematical modeling in science and applied fields, and even in medicine. The most generally used is the Finite Element Method (FEM) which also is the basic methodology of this report.

This paper aims to emphasize the generality of the Kojic Transport Model (KTM) which is based on the concept of smeared physical fields in biomedical engineering. The KTM has a strong distinction from other approaches and we first refer to a few references which illustrate this distinction. This way we also provide an insight into the advantages and generality of our methodology.

In [2] it is introduced an n-compartment mammillary distributed-parameter model for the estimation of physiological parameters in tumors, such as perfusion, mean transit time, fractional volumes, and transfer and rate constants. The idea consists of the division of the tumor's space into the capillary compartment to which other compartments, called the peripheral interstitial compartments, are connected. The diffusion of the tracer is governed by the convective-diffusive mass balance equations within the capillary, while diffusion only is taken within the compartments. Mass transport within the capillary of a length L is given by the following convective-diffusion equation

$$r_{V1}\frac{\partial c_1}{\partial t}+Q\rho L\frac{\partial c_1}{\partial x}+\sum_{i=2}^{n}K_{i1}c_1-\sum_{i=2}^{n}K_{1i}c_i=Lq_V \tag{1}$$

while diffusion within compartments is governed by equations

$$r_{Vi}\frac{\partial c_i}{\partial t}+K_{1i}c_i-K_{i1}c_1=0 \quad i=2,.....,n \tag{2}$$

where c_1 and c_i are concentrations; r_{V1} and r_{Vi} are volumetric fractions within capillary and compartments, respectively; Q is volumetric flux per unit mass of tissue within the capillary, ρ is transported mass density; K_{i1} and $K1i$ are transport coefficients from capillary to the compartment and vice-versa; and q_V is a volumetric term associated with capillary. Equations (1) and (2) are solved in analytical form by the integral Laplace transformation and results are fitted to the experimental data to obtain material coefficients.

Another example that is related to the KTM is the determination of perfusion within an arterial blood vessel of the heart [3,4]. These authors introduced compartments for arterial blood vessels according to the lengths and diameters of capillaries within reference volumes around selected points within the heart tissue wall. The governing equations for blood flow within a compartment i have a usual form based on the Darcy law,

$$v_j^{(i)}=k_{Djk}^{(i)}p_{,k} \quad i=1,2,..,N;\ j,k=1,2,3 \tag{3}$$

and the mass balance equation is

$$v_{j,j}^{(i)}=s^{(i)}-\sum_{k=1}^{N}\beta_k^{(i)}(p_i-p_k) \tag{4}$$

where $v_j^{(i)}$ are Darcy velocities, $k_{Djk}^{(i)}$ is Darcy permeability tensor, p is pressure, $p_{,k}\equiv\partial p/\partial x_k$, $s^{(i)}$ is a source term, and $\beta_k^{(i)}$ are inter-compartment coupling (transport) coefficients. The capillary flow is represented in a continuum form by a permeability tensor evaluated within a reference volume. This tensor is analogous to our transport tensor given in the next section. Volumetric participations within compartments are taken into account by specifying a continuum porosity. The same approach to modeling perfusion is applied in Ref. [5].

Finally, we in this section refer to the modeling of electrical signal propagation in heart electrophysiology. The so-called phenomenological models are continuum models which can be compared with our KTM methodology. There are two types of these – initial monodomain followed by bidomain model. In the case of the monodomain model, the membrane potential (difference between cell internal and external electrical potentials) field is determined taking into account ionic fluxes through membranes and the volumetric fraction of the cells. We here give the fundamental balance equations for current density in the case of a bidomain model, called the extended bidomain model, according to Ref. [6]. The model includes two cell groups, group 1 and group 2, with their conduction characteristics, and the equations are, according to the notation used in our KTM representation,

$$-r_{AV}^{(1)}\frac{\partial}{\partial x_i}\left[C_m^{(1)}\left(\frac{\partial V_e^{(1)}}{\partial t}-\frac{\partial V_e^{(ext)}}{\partial t}\right)+I_{ion}^{(1)}\right]+\frac{\partial}{\partial x_i}\left(G^{(1)}\frac{\partial V_e^{(1)}}{\partial x_i}\right)=0\ -r_{AV}^{(2)}\frac{\partial}{\partial x_i}\left[C_m^{(2)}\left(\frac{\partial V_e^{(2)}}{\partial t}\right.\right.$$
$$\left.\left.-\frac{\partial V_e^{(ext)}}{\partial t}\right)+I_{ion}^{(2)}\right]+\frac{\partial}{\partial x_i}\left(G^{(2)}\frac{\partial V_e^{(2)}}{\partial x_i}\right)=0\ \frac{\partial}{\partial x_i}\left(G^{(1)}\frac{\partial V_e^{(1)}}{\partial x_i}\right)+\frac{\partial}{\partial x_i}\left(G^{(2)}\frac{\partial V_e^{(2)}}{\partial x_i}\right)+\frac{\partial}{\partial x_i}\left(G^{(ext)}\frac{\partial V_e^{(ext)}}{\partial x_i}\right)=0 \quad (5)$$

where the upper indices 1 and 2 correspond to the first and second group of cells, while 'ext' stands for the extracellular space; r_{AV} is the area-to-volume ratio for cells; C_m is membrane electrical capacitance; G is electrical conductivity for cells and extracellular space, respectively; I_{ion} is ionic membrane flux, and V_e is electrical potential within cells and extracellular space.

2. Methodology

2.1. Gradient-driven physical fields and Kojic transport model (KTM)

Here we summarize the FE formulation according to Ref. [7]. Application of this methodology is given in a number of our references [8–17], and is described and summarized in Ref. [1]. This methodology is built into our FE software package PAK-BIO [18]. The background of the smeared concept and the KTM formulation of the composite smeared finite element (CSFE) are shown in Fig. 1. We further summarize the formulation of this element.

First, we note that gradient-driven physical fields of interest in biomedical engineering considered here, are governed by a gradient law

$$J_i=-D_{ij}\frac{\partial\varphi}{\partial x_j}, i,j=1,2,3; \quad sum\ on\ j \quad (6)$$

where $\varphi(x_i,t)$ is the physical field depending on spatial coordinates x_i and time t, J_i is the flux of φ (per unit surface and unit time), and D_{ij} is the constitutive transport tensor. The fundamental balance equation, which has to be satisfied at any spatial point and any time for the field, can be written in the following form,

$$-c\frac{\partial\varphi}{\partial t}+\frac{\partial}{\partial x_i}\left(D_{ij}\frac{\partial\varphi}{\partial x_j}\right)+q_V=0, sum\ on\ i\ and\ j \quad (7)$$

where c is the rate coefficient, and q_V is the source term representing the rate of φ per unit volume. For diffusion, the rate coefficient is $c = 1$ and φ is concentration; $c=\rho c_T$ for heat transfer, where ρ is density, c_T is specific heat and φ is temperature; c = 0 for flow through porous media and φ is pressure. Transport tensor is the diffusion tensor, heat conduction tensor, and Darcy's tensor - for diffusion, heat transfer, and flow through porous media, respectively. In the case of electrical conduction, equation (6) is applicable, where J_i is

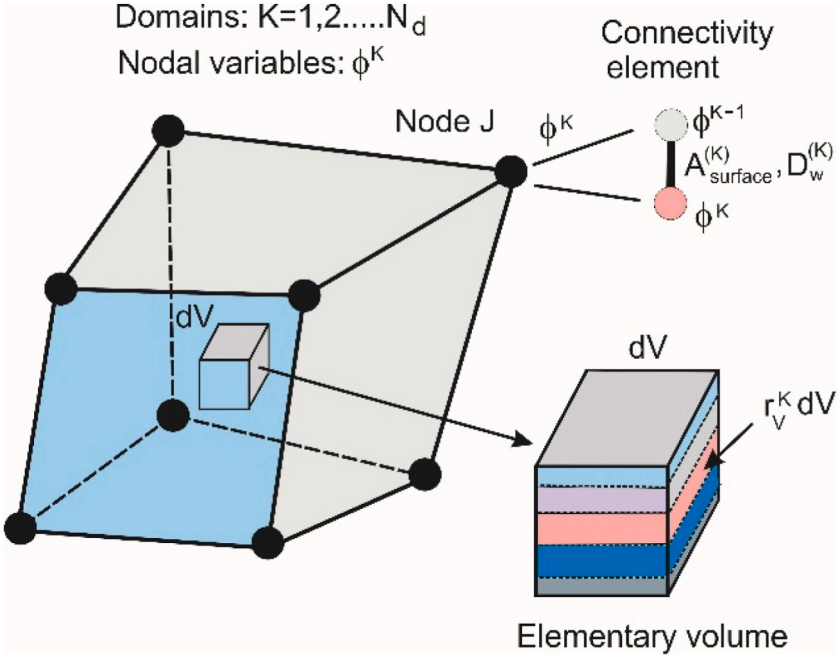

Fig. 1. Composite smeared finite element (CSFE) with coupled physical fields within volumetric domains occupying the element space. According to Ref. [7].

current density, D_{ij} is a diagonal conductivity tensor and φ is electrical potential. The above equations correspond to a general 3D or 2D continuum space, but they can be reduced to the 1D conditions which are present in biological systems as flow or mass or transport within small vessels, or electrical signal propagation by nerve network.

The important step in the formulation of the CSFE is a transformation of the 1D transport equations to a continuum form to treat the 1D transport as in other continuum domains within the CSFE. This is achieved by a consistent derivation of the expression for the transport tensor [1], which can be written as

$$D_{ij} = \frac{1}{A_{tot}} \sum_K D_K A_K \ell_{Ki} \ell_{Kj} \tag{8}$$

where D_K is the transport coefficient of a K-th 1D structural element in the vicinity of a considered spatial point of the physical field; A_K are cross-sectional areas of the elements, A_{tot} is the sum of all A_K, and ℓ_{Ki} are directional cosines of the 1D elements. This detail in the KTM contributes not only to the generality but also to simplicity in applications. An analogous expression to our expression in equation (8) is used in Refs. [3,4], equation (3).

The continuum balance equation (7) are further transformed into the FE format for each domain by a standard Galerkin method [1]. These balance equations for each domain K, a time step of size Δt, and equilibrium iteration i can be written as,

$$\left(\frac{1}{\Delta t}\mathbf{M} + \mathbf{K}\right)^{(i-1)} \Delta\mathbf{\Phi}^{(i)} = \mathbf{Q}^{ext(i-1)} + \mathbf{Q}_V^{(i-1)} - \left(\frac{1}{\Delta t}\mathbf{M} + \mathbf{K}\right)^{(i-1)} \mathbf{\Phi}^{(i-1)} + \frac{1}{\Delta t}\mathbf{M}\mathbf{\Phi}^t \tag{9}$$

where element matrices $\mathbf{M}$ and $\mathbf{K}$ take into account transitional and transport characteristics, while $\mathbf{Q}^{ext(i-1)}$ and $\mathbf{Q}_V^{(i-1)}$ are external (to the element) and volumetric fluxes; and $\mathbf{\Phi}^{(i)}$, $\Delta\mathbf{\Phi}^{(i)}$ and $\mathbf{\Phi}^t$ are nodal vectors, nodal increments, and vectors at the start of a time step, respectively. The specificity of the matrices and nodal vectors is that they include the volumetric fractions of the domains. For example, the transport matrix $\mathbf{K}$ for a domain K is

$$K_{IJ}^K = \int_V r_V^K D_{ij}^K \frac{\partial N_I}{\partial x_i} \frac{\partial N_J}{\partial x_j} dV, \; sum \; on \; i,j; \; i,j = 1,2,3 \tag{10}$$

where r_V^K is the volumetric fraction, and N_I, N_J are the FE interpolation functions.

A very important step in the formulation of the CSFE is how to couple mutually dependent physical fields within the continuum domains. This is achieved by introducing connectivity elements at each FE node. There are as many of these elements at a node as there are the coupling of the fields. Moreover, these practically fictitious elements represent biological barriers as capillary walls or cell membranes. The balance equation for a connectivity element at node J between domains m and n is (dropping out the rate terms)

$$K_{wIJ}^{m,n} \Delta\Phi_J = -K_{wIJ}^{m,n} \Phi_J, I, J = 1,2 \tag{11}$$

where the connectivity matrix $K_{wIJ}^{m,n}$ is

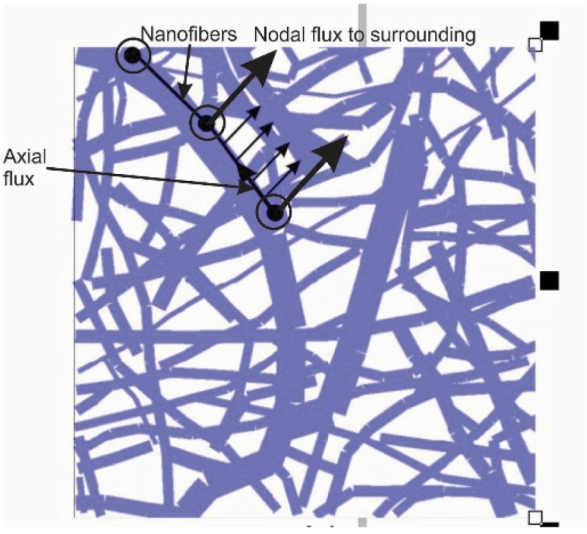

Fig. 2. Image of nanofiber network with axial diffusion with fibers and radial diffusion to the surrounding. Lab of the Faculty of Technology and Metallurgy, University of Belgrade, Serbia [15,16].

$$K_{wIJ}^{m,n} = r_V r_{AV} D_w V_{node} \begin{bmatrix} 1 & -1 \\ -1 & 1 \end{bmatrix} \tag{12}$$

In the above equations (11) and (12), r_V, r_{AV}, D_w and V_{node} are the nodal values of the volumetric fraction, area-to-volume coefficient, wall transport coefficient, and volume (of the FE assembly) belonging to the node, respectively. The area coefficient is $r_{AV} = 4/d_{cap}$ for capillaries with d_{cap} being the capillary diameter, while for spherical cells with diameter d_{cell}, it is $r_{AV} = 6/d_{cell}$.

To illustrate the KTM generality, here is given application to modeling mass release from a nanofiber network to the surrounding. This process is particularly suitable for medical implants where the drug release to tissue can be adjusted. Using electrospinning, it is possible to generate a nanofiber network containing a certain concentration of drug which is released by diffusion to the surroundings. An image of these nanofibers is shown in Fig. 2.

The axial diffusion along the fibers is transformed to the continuum format as for the other 1D structures, with the evaluation of the diffusion tensor according to equation (8), while the governing balance equation has the form (9). The drug release from the fibers is achieved by connectivity elements (displaced in Fig. 2) according to the FE balance equation (9), with the matrices (for a node J)

$$\begin{aligned} &M_{11} = \frac{1}{3} A_{fibJ} R_J, M_{21} = \frac{1}{6} A_{fibJ} R_J, M_{12} = P_J M_{21}, M_{22} = P_J M_{11} \\ &K_{11} = -K_{21} = A_{fibJ} D_{fibJ}, K_{22} = -K_{12} = P_J\ K_{11} \end{aligned} \tag{13}$$

In this equation (13) R_J is the fiber radius; P_J and D_{fibJ} are partitioning and diffusion coefficient, respectively; and $A_{fibJ} = (r_V r_{AV} V)_J$, where $(r_{AV})_J = 2/R_J$ is the area-to-volume ratio and V_J is the volume of the continuum belonging to node J.

The accuracy of this model is assessed by comparing the KTM solution with that obtained using the model with specific composite finite elements for fibers [11].

2.2. The generality of the KTM and comparison with other methods

In this section, we summarize the generality of the KTM and then give some evidence of the advantages of our computational models compared to other methodologies for the gradient-driven physical fields within biological systems.

In the previous section, we presented the fundamental assumptions in the formulation of the CSFE. Following that, we can emphasize several key facts which illustrate the generality of the KTM.

1) The KTM, based on the multiscale composite finite element (CSFE) with smeared fields, can be considered a new avenue that offers a simple straightforward consistent formulation for modeling gradient-driven physical fields in biological systems.
2) The CSFE is a continuum multiscale finite element composed of different physical fields (domains) which are mutually dependent. These domains have different spatial scales from macro to nanoscale. For example, the physical fields are related to the mass

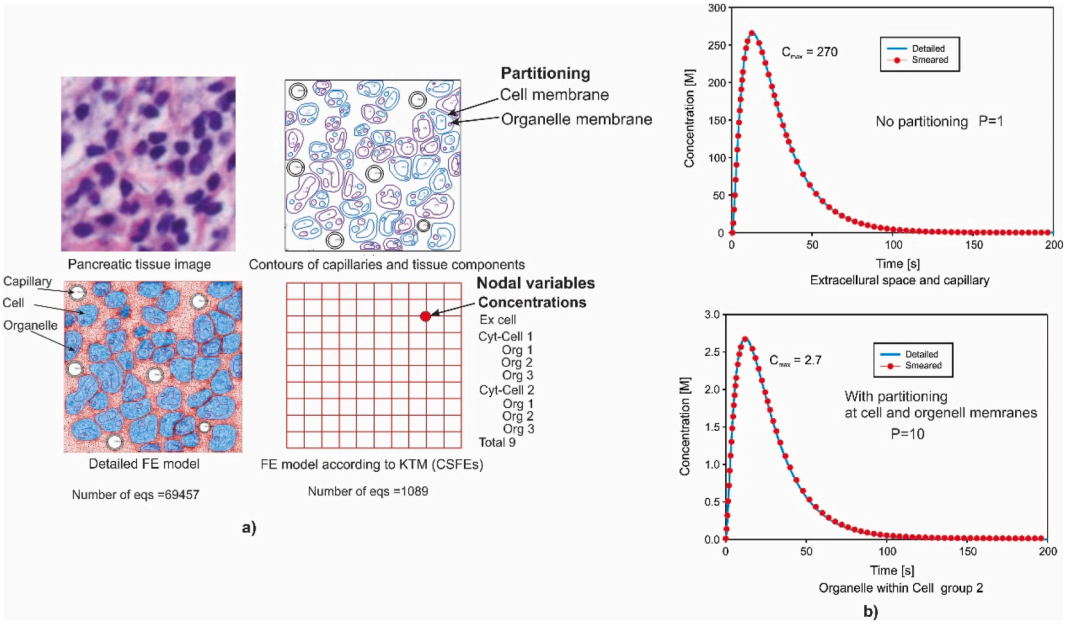

Fig. 3. a) Image of a 50x50 μm tissue domain of pancreatic cancer, contours of two groups of cells with two organelles (upper panel); detailed 2D FE model of tissue with 6 capillaries normal to the image plane, and simple model with CSFE (lower panel). b) Mean concentration evolution within capillaries (prescribed) and in extracellular space (upper panel), and organelles of Cell group 2 – with partitioning (lower panel). According to Ref. [12] with small modifications.

transport from capillaries through capillary walls, to extracellular space, further through cell membranes to cell interior cytosol, and through organelle membranes to the organelle interior. In applications, we have used the same time steps within the models, but a subdivision of the time step for lower scales can simply be employed.

3) The 1D detailed models, with the use of 1D finite elements to follow the networks within which the process (transport) occurs, as in capillaries, neural networks, or nanofibers, are applicable to small spatial domains due to the complexity of geometry and the requirement of huge effort for model generation. On the other hand, our equivalent 3D continuum models are simple for space discretization and need appropriate transport tensor evaluation according to (8). This tensor can be associated with FE nodes to take the heterogeneity of parameters within the space.
4) The accuracy of the KTM model has been assessed in a number of our publications, summarized in Ref. [1]. The original formulation was improved by correction functions introduced in Refs. [15,16], here illustrated in solutions in Fig. 3. Generally, the smeared physical fields can be considered as the mean value solutions in a vicinity of a considered spatial point.
5) The KTM generality is particularly notable in modeling the biological barriers between the continuum domains. We illustrate the effects of partitioning at the biological barrier interfaces in an example following solutions in Ref. [12]. Fig. 3a shows detailed and the KTM FE models where we can see that the detailed model, with the use of standard 2D FEs, leads to 69,457 equations to be solved, while the KTM model, with the use of only 100 CSFEs, has 1089 equations. The reduction in the number of equations is around 70 times, hence the efficiency is increased by approximately the same number. It is assumed a bolus-type prescribed concentration within capillaries and concentration fields are calculated within two types of cells and organelles. Fig. 3b shows solutions for the mean concentrations in the

extracellular space (upper panel) and organelles (lower panel). It can be seen a 100 times reduction of concentration within organelles due to partitioning (partitioning coefficient at the cell and organelle equal to 10). This effect of partitioning is a measure of hydrophobicity important in drug delivery. Other solutions are given in Ref. [1].

This example illustrates the generality of the KTM by including the hydrophobicity of molecules at the biological barriers, as well as the accuracy of the KTM since practically there is no difference between the two solutions in Fig. 3b.

By comparing our concept of connectivity elements with, for example, the approach given in Ref. [2], it can be seen that in equation (2) there is no explicit measure of the surface at a FE node through which the transfer from capillary occurs - as we have in expressions (13). The same conclusion can be drawn when comparing our connectivity elements with expressions (4) of reference [3,4]. Other specific molecular processes occurring at the cell membranes and within cells, which are fundamental for drug delivery, can be incorporated straightforwardly into our connectivity elements and continuum subdomains. For example, specific properties of the functionalization of nanoparticle surfaces [19], can be included. Or, the kinetics of the ligand-receptor binding can be incorporated. This kinetics, according to Ref. [20], is described by equation (14) of molecular interactions,

$$\begin{aligned}\frac{dC_b}{dt} &= k_a C_{bs} C - k_d C_b - k_{\text{int}} C_b \\ \frac{dC_{bs}}{dt} &= -k_a C_{bs} C + k_d C_b + R_s \\ \frac{dC_i}{dt} &= k_{\text{int}} C_b\end{aligned} \tag{14}$$

where C_{bs}, C_b, C_i, and C are concentrations of unbound binding sites, bound vesicles, internalized vesicles, and free vesicles per tumor volume, respectively; k_a, k_d, and k_{int} are the association, dissociation, and internalization rate constants, respectively; and R_s is synthesis rate of new binding sites.

6) Further, we refer to models applied in electrophysiology. A detailed comparison of the traditional bidomain models, as the one described by equation (5), and the KTM, is given in Refs. [1,14]. We here notify few of the differences between our and traditional models. Unlike the previous models which consider the entire continuum without compartments with their own volumes, in the KTM we treat each compartment separately with their specific transport properties. The physical fields are computed within the compartments, organized in a natural way and hierarchically according to the transport process; the fields are connected by the appropriate connectivity elements. As stated earlier, the connectivity elements represent biological barriers, and in the case of electrophysiology they specify the conductances from the neural fibers to the surrounding, and through cell membranes. According to the KTM, the governing balance equations refer to each tissue domain separately, with the volumetric fractions r_V^K (K is compartment number), while in the previous models they correspond to the entire continuum, e.g. equation (5). The KTM hierarchy and multiscale character can be seen from the expression for the volume of a cell subdomain (here given by equation (15)):

$$V_N^k = r_V^k r_V^N V \tag{15}$$

where r_N^k is the relative volume ratio of the subdomain with respect to the cell volume, whose ratio r_V^N is related to the finite element volume V. Accuracy of the KTM is demonstrated and assessed by comparison with respect to the detailed FE models of a composite tissue [1,8–13].

Finally, we indicate applications of the KTM which are not considered in our publications. The first example is related to an extension of our models to heart perfusion where blood vessels larger than capillaries are classified according to their diameters. The

corresponding CSFE is shown in Fig. 4. Besides perfusion, the model may also include mass transport by diffusion and.

electrical field. Our model has advantages with respect to the multi-compartment Darcy perfusion models of [3–5], as already discussed, but also it is more general.

The second example of further application of the KTM is related to mass transport within the lungs. The concept of this model is shown in Fig. 5. The model assumes coupled mechanics and mass transport (airflow and diffusion). The lung function involves a large change of the lung geometry, therefore the airways within parenchyma are subjected to significant cyclic changes in size over breathing cycles. For mechanics, 1D finite elements can be used for large airways, while for parenchyma 3D FEs with internal microstructure [21] may be implemented. Regarding mass transport – airflow and particulate transport by diffusion, 1D or 3D FEs can be employed for large airways. The parenchyma consists of small airways classified as airway generations and KTM applies, with equivalent 3D domains for each generation or a group of generations. A transport matrix $K_{Jk,k+1}$ at node J between two domains, k and $k+1$, can be expressed in a form given in Fig. 5, where D_{Jk+1} and V_{Jk+1} are transport coefficient and continuum volume of the domain $k+1$ belonging to the node, respectively. We give the first results of this model in the next section.

2.3. *A few selected examples for demonstrating the generality of the KTM*

In this section, we have selected a few examples from our earlier publications to illustrate the statements on the generality of the KTM.

Fig. 6a and b show the modeling of mass release from a nanoparticle according to Ref. [22]. The goal was to find the effective partitioning coefficient for the release of molecule Rhodamine B from a.

nanoparticle to its surroundings. The partitioning coefficient as a measure of hydrophobicity is further built in our KTM models. As stated in Section 2.1, it is an important feature for the KTM that partitioning is included in the connectivity elements for any boundary between the domains (e.g. vessel walls or membranes). The 2x2 connectivity matrix is modified to include partitioning according to (13).

Another example demonstrates the application of the KTM to large-scale models. In Ref. [13]) it was considered mass transport in the pancreas when a bolus-type entering of mass occurs in the pancreas main artery. A constant pressure is assumed at the entrance. The model is generated from imaging data obtained at a lab in MD Anderson Cancer Center in Houston. The model includes large blood vessels, capillary system, lymphatic system, extracellular space, and two types of cells with their organelles. There are 7 continuum subdomains with their volumetric fractions, diffusion characteristics, and partitioning at cell and organelle membranes. Each node has 10 variables – 3 pressures and 7 concentrations. The number of equations to be solved is 1,025,502. Other details are given in reference [13]. In Fig. 7 are shown.

concentration fields in different domains, where differences can be noticed due to partitioning effects. Fig. 8 shows the evolution of the mean concentration in different domains which also demonstrates the effects of the diffusion and partitioning characteristics.

We further give an example that shows an application of the KTM to the diffusion of ions (charged molecules), where we have a coupling of electrical and concentration fields [14]. The mass balance equation here includes concentration and electrical potential,

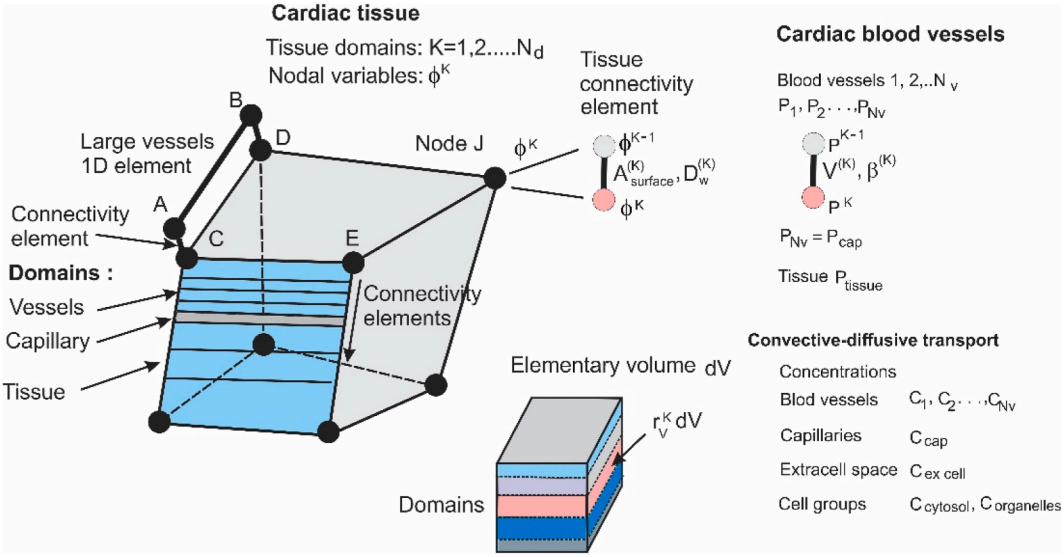

Fig. 4. Composite smeared finite element (CSFE) with subdomains for cardiac blood vessels classified according to vessel diameters. The first equivalent continuum vessel domain is connected to 1D large vessel network, while the last is connected to the capillary continuum domain. Tissue nodal variables φ^k may include pressure, concentration, and electrical potential.

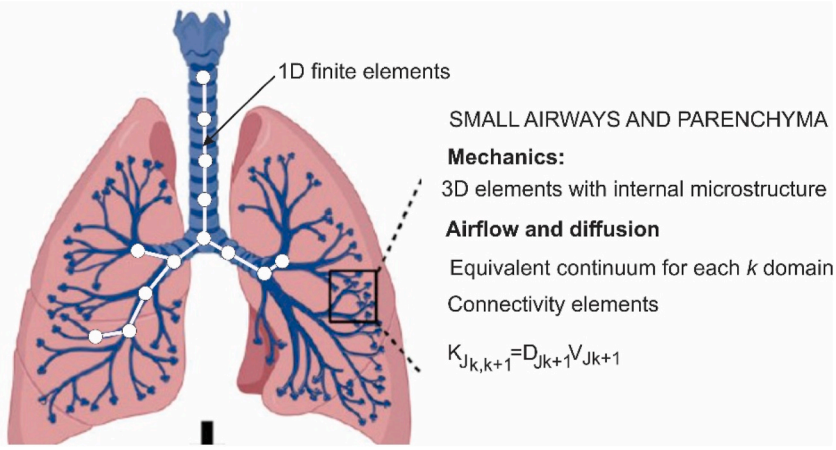

Fig. 5. A FE model for lung mechanics, airflow, and diffusion. Mechanics: 1D, and a multiscale 3D continuum FEs with internal microstructure [21]. Mass transport: 1D and KTM for large airways and parenchyma.

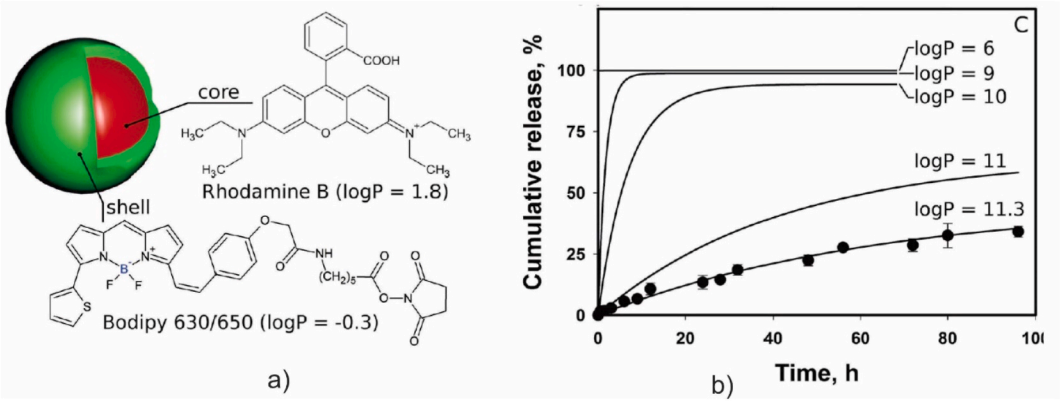

Fig. 6. Determination of the effective partitioning coefficient for the release of Rhodamine B from a nanoparticle to the surrounding (According to Ref. [22]).

$$\frac{\partial c^m}{\partial t}=\frac{\partial}{\partial x_i}\left[D\frac{\partial c^m}{\partial x_i}+\frac{Dz^mF}{RT}c^m\frac{\partial V_e}{\partial x_i}\right], sum\ on\ i: i=1,2,3 \tag{16}$$

where c^m is the concentration of ion m, V_e is the electrical potential, D is the diffusion coefficient, z^m is molecule valence, F is the Faraday constant, T is the absolute temperature, and R is the universal gas constant. To illustrate the generality of the KTM we show schematics of connectivity elements in case of electrical conduction through nerves and cell membranes (Fig. 9a and b)

We modeled a tissue sample of the shape as in Fig. 3, isolated and with 6 neural fibers normal to the plane using a detailed 2D model and the KTM model. It was assumed that there are two groups of cells, that electrical potential in fibers is constant, and that there are ionic currents of potassium and sodium through cell membranes (details are given in Ref. [14]). The evolution of electrical potential within extracellular space and cells is shown in Fig. 10.

Finally, we show in this section one of the results recently obtained to be used for lung modeling according to Fig. 5. Fig. 11 shows a model of airflow that includes a 3D/2D axisymmetric domain connected to 1D pipe elements immersed within a 3D domain of lung parenchyma. The first FE domain is based on the Navier-Stokes equations, while the second domain is modeled by 1D pipe elements connected to our general lung multiscale-multiphysics FEs (GLFEs). It is taken that air velocities and concentrations are given on the left side of the fluid domain, while zero pressure and zero concentrations are specified for 1D pipe elements on the right boundary. We here give (Fig. 12a and b) a change with time of concentration within pipe elements and at a point within the parenchyma. Details of the model and other solutions are given in the cited reference.

3. Results – additional examples

Application of the KTM has been demonstrated in a number of our publications, with a few examples in Section 2.3, while a summary is provided in the book [1]. Here, we present solutions for two new examples – one related to molecular convective-diffusive

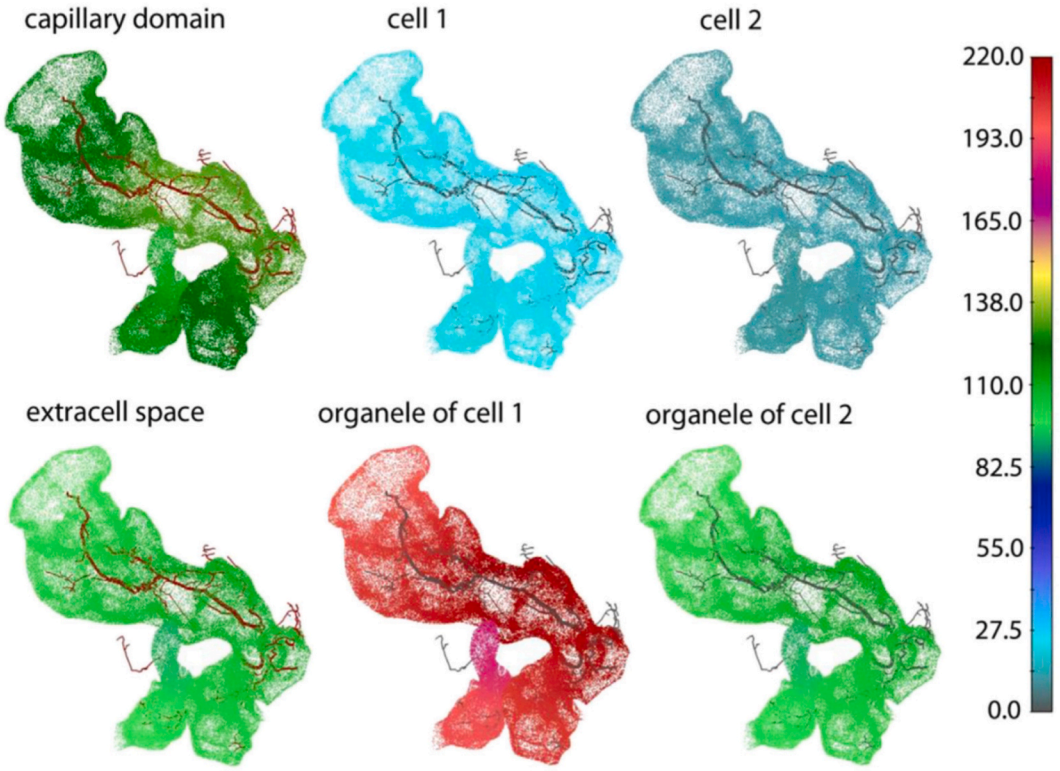

Fig. 7. Concentration fields within the pancreas at time t = 20s. Concentration for the Cell 2 group (portioning P = 10 at cell membrane) is significantly smaller than for Cell 1 (P = 5) due to partitioning. (According to Ref. [13]).

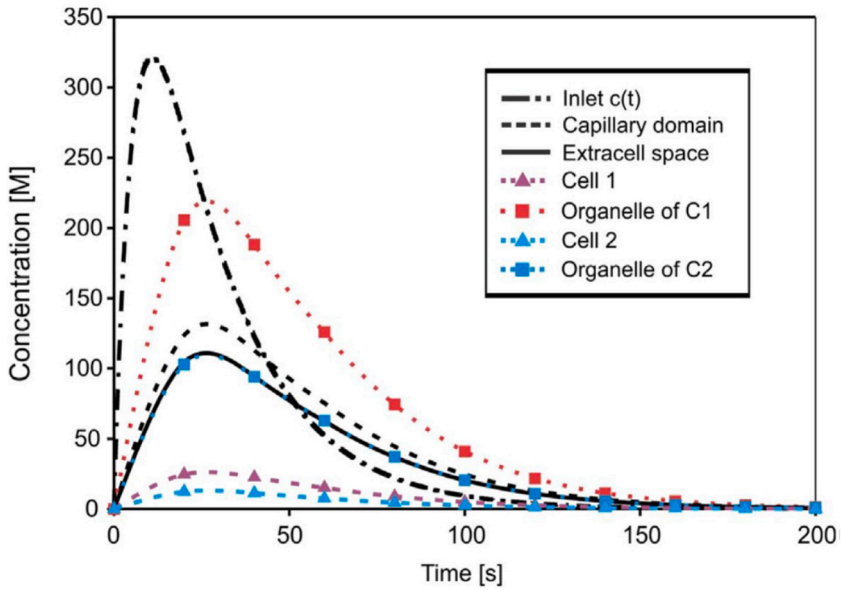

Fig. 8. Evolution of concentration in different domains of the pancreas (According to Ref. [13]).

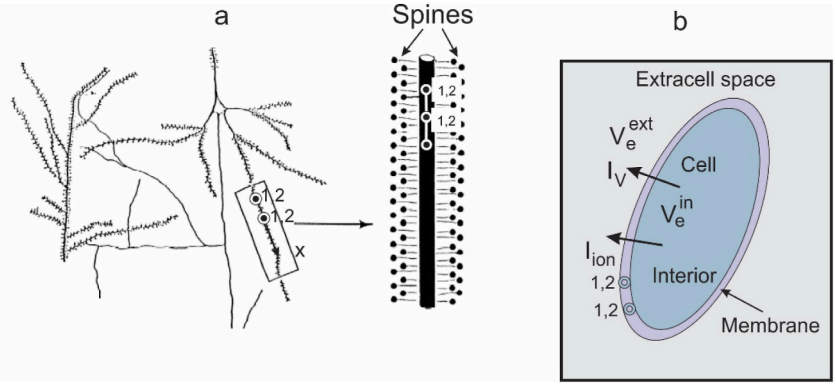

Fig. 9. Schematic of nerve fibers and cells. a) Dendritic tree and 1D finite elements along the nerve fibers with connectivity elements 1,2; b) Cell with current I_V through membrane due to potential difference membrane, and ionic current I_{ion} due to molecule flow modeled by connectivity elements 1,2. (According to Ref. [14]).

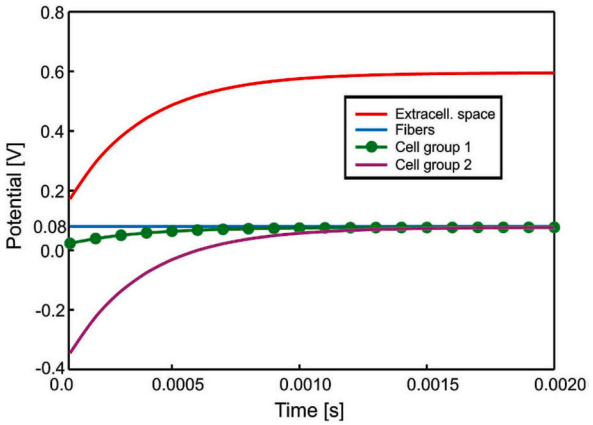

Fig. 10. Evolution of the mean potential in extracellular space and cells, detailed
and smeared solutions; with ionic currents of potassium and sodium included. (According to Ref. [14]).

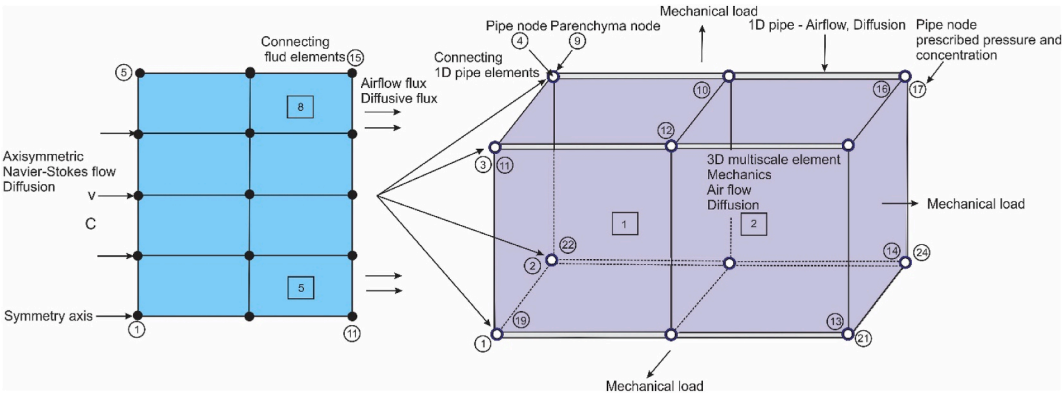

Fig. 11. Two models coupled - 3D or axisymmetric fluid domain (left) coupled to 1D (pipe) model within a 3D parenchyma model (3D GLFE elements). Boundary fluid elements 5–8 are connected to boundary pipe nodes 3,4,19,22. (According to Ref. [23]).

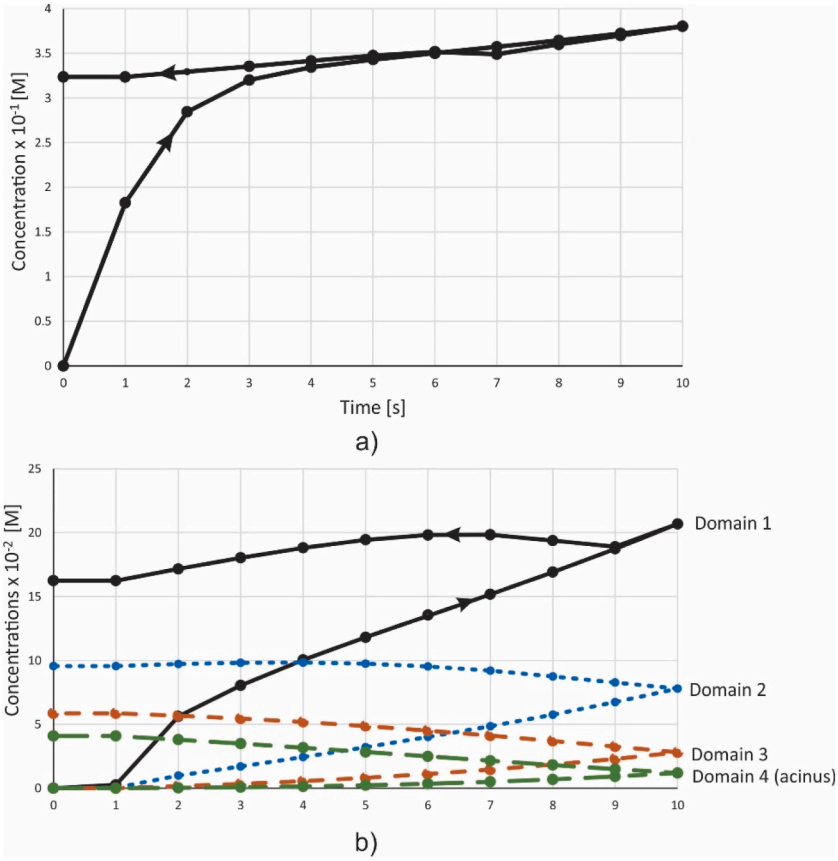

Fig. 12. a) Concentration at the connection of pipes with fluid over time; b) Concentration over time at a point close to pipe connection with fluid, for the small airway domains. (According to Ref. [23]).

transport within a tumor, and another shows computation of drug delivery from nanofibers.

3.1. Convective-diffusive transport within a tumor

Data for this model comes from a laboratory from the Department of Nanomedicine at Houston Methodist Institute. A tumor growth within a mouse is recorded and we consider a middle cross-section for which data for the geometry, capillary distribution and diameters, and volumetric fraction of cells are provided during the tumor evolution. The data are assigned to a 10x10 regular mesh from which are calculated values for the finite element mesh. Using these data a study of perfusion is considered in Ref. [24]**.** Here, we extend that analysis to include diffusion. The data used in this example are:

Volumetric fractions of capillaries and cells – nodal variable dependent on deformation, input from imaging data;

Darcy tensor (diagonal): $k_{Dii} = 1e^{-2}$ [mm^2/(Pa s)];

The hydraulic coefficient for the capillary wall: h = 12.5 [ml/min/mmHg];

Diffusion tensor for extracellular space and cells (diagonal): $D_{ii} = 1$ [mm^2/s];

Diffusion transport coefficient for capillary wall and cell membrane: $D_w = 1$ [mm/s].

It is taken that the pressure in capillaries is uniform and constant, equal to 10 mmHg, while the concentration of transported drug molecules has a bolus shape as shown in Fig. 14. It is adopted that both pressure and concentration in the extracellular space at the tumor boundary are equal to zero. On the other hand, it is taken that there is no diffusion at the boundary between cells within the tumor and surrounding tissue.

Fig. 13 shows concentration fields at the initial position, and final configuration, at the time $t_{max} = 12$s, when the concentration within capillaries reaches a maximum (at each configuration). It can be seen that concentrations are quite uniform within both extracellular and cell domains, with significantly smaller values within cells. This difference comes from diffusion as a time-dependent process.

Fig. 14a displays the mean concentration over time for the extracellular space and cells, while Fig. 14b and c shows concentration distibutions along the x-x line in Fig. 13. It can be seen that concentration within the extracellular space is smaller than in the capillaries and further decreases in the cells. Also, a hindrance of the concentration maximum can be noticed between these curves. These effects result from the presence of capillary walls and cell membranes as biological barriers. Fig. 15(a–c) show the results as in Fig. 14,

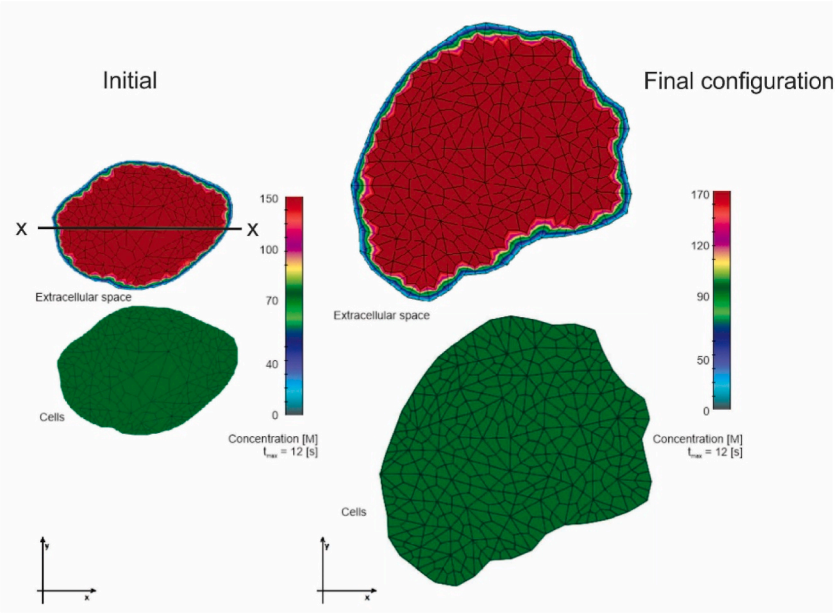

Fig. 13. Concentration fields at initial and final configurations, time is $t_{max} = 12$s when the bolus of capillary concentration reaches the maximum (shown in Fig. 14).

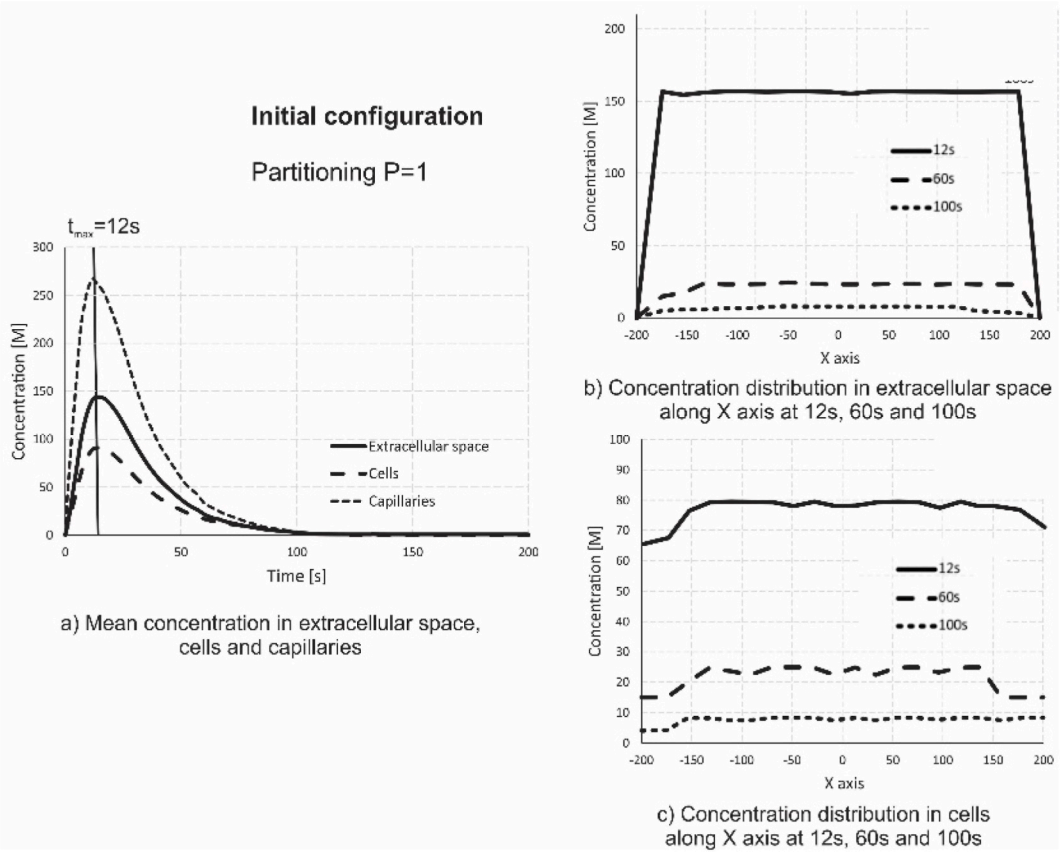

Fig. 14. a) Mean concentration over time for capillaries, extracellular space, and cells; b), c) Distribution of concentration along the x-x line (Fig. 13) for extracellular space and cells at three times. No partitioning.

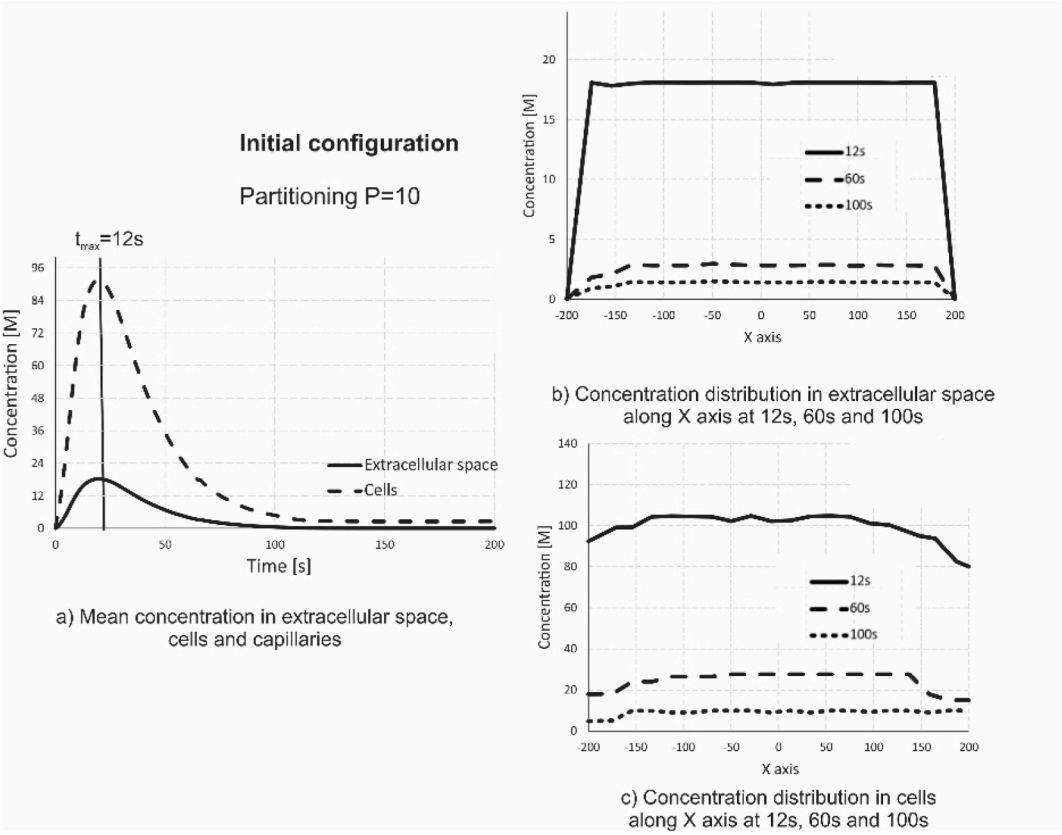

Fig. 15. Initial configuration. a) Mean concentration over time for extracellular space and cells; b), c) Distribution of concentration along the x-x line (Fig. 13) for extracellular space and cells at three times. Partitioning between capillary walls and extracellular space, P = 10.

but assuming that there is a partitioning (effect of hydrophobicity) at the interface between the capillary wall and extracellular space. It is taken that the partitioning coefficient is P = 10. Now, concentrations within extracellular space and cells are reduced due to partitioning.

Finally, in Fig. 16a-c we show the results as in Fig. 15, but for the final configuration. It can be seen that the solutions at these two figures have the same character, hence the change of geometrical data and other model parameters affect mainly the values of concentration. The same findings apply to the case with partitioning P = 10 (results not shown).

3.2. *Drug delivery from nanofibers*

We modeled drug delivery from nanofibers in our previous publications ([1,15–17]). Here we extend these models to the investigations of the effects of degradation and hydrophobicity on drug release.

The drug release from nanofibers has been thoroughly studied experimentally, and here are cited some of these studies. Poly (D, L-lactic-*co*-glycolic acid) - (PLGA) is the most commonly used polymer to create 3D scaffolds in tissue engineering [25,26]. PLGA can be prepared in several forms according to the different ratios of its constituents, lactic (LA) and glycolic acid (GA). It has been shown that the rate of degradation (i.e. the weight loss of polymer) is affected by the percentage of glycolic acid (GA) in PLGA [27,28], where the fastest degradation occurs for PLGA 50:50 (LA/GA) and the slowest for PLGA 85:15 (LA/GA). We here consider a model for a three-layer PCL/PLGA/PCL implant shown in Fig. 17a, as in Ref. [17], with the corresponding equations for mass transport and degradation, and the LA/GA ratio of 50:50, 65:35, 75:25, and 85:15. According to the measurements [17] we used the volume fraction (rV) of nanofibers of 78% for PLGA 50:50 and 59% for PLGA 65:35, while for PLGA 75:25 and PLGA 85:15, the porosities were 50% and 43%, respectively. Based on the data from Ref. [28], we use the following parameters for hydrophobicity (higher partitioning coefficient means lower hydrophobicity) in the numerical simulation: $P = 1 \times 10^{-5}$ (50:50), 1×10^{-6} (65:35), 5×10^{-7} (75:25), and 1×10^{-7} (85:15). These data are in accordance with the findings in Ref. [29] that larger presence of GA in PLGA reduces the degradability of the polymer and increases hydrophobicity. The following values were used for coefficients of degradation: $\kappa_w = 2.5 \times 10^{-7}$ (50:50), 2.0×10^{-7} (65:35), 1.5×10^{-7} (75:25), and 1×10^{-7} (85:15) s^{-1}.

Concentration fields within the fibers of the PCL/PLGA/PCL scaffold at time t = 50 days are shown in Fig. 17b. Mass release curves in the case of the RhB complex impregnated into standard PLGA complexes: 50:50, 65:35, 75:25, are shown in Fig. 17c. It can be noticed that drug release increases with a decrease of the PLGA ratio, which can be attributed to an increased mass loss due to

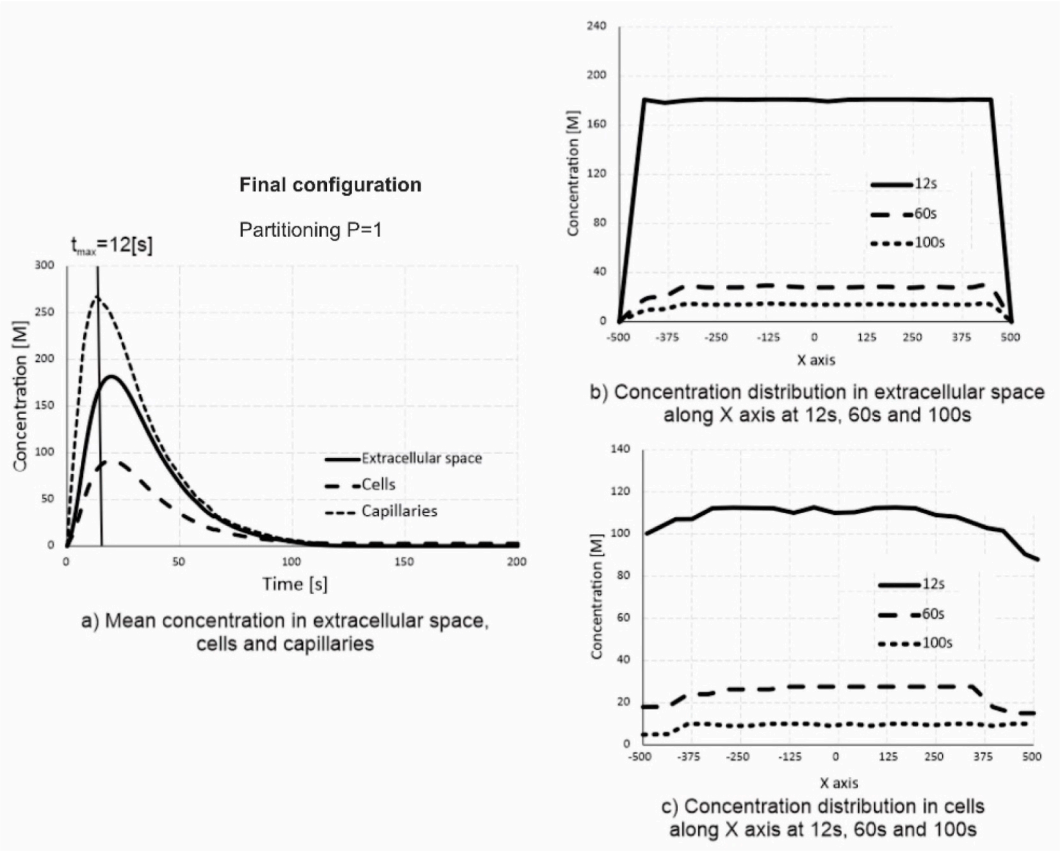

Fig. 16. Final configuration. a) Mean concentration over time for extracellular space and cells; b), c) Distribution of concentration along the x-x line (Fig. 13) for extracellular space and cells at three times. Partitioning between capillary walls and extracellular space, P = 10.

degradation and decreased hydrophobicity. Dependence of the mass release on the fiber density within the math, expressed by the volumetric fraction r_V of the fibers, is shown in Fig. 17d, for several values of the r_V: 0.2, 0.3, 0.423, 0.5, and 0.6. The results show that the mass release is faster when the fiber density is smaller. This occurs because the effective diffusion coefficient increases with a decrease of the fiber density. Namely, during diffusion within a porous medium, there exists the interaction between the solid phase (here fibers) and transported molecules width reduced diffusivity. This phenomenon was analyzed and quantified in Ref. [1] (Chapter 5), and [30]. The effective diffusion coefficients for the PCL layer were found to be: $D_{equiv} = 0.008$, 0.0071, 0.006, 0.0053, and 0.0044 μm2/s, for the volumetric fractions of rV = 0.2, 0.3, 0.423, 0.5, and 0.6, respectively. It was assumed that the diameter of the fibers in the PCL layer is the same for all three cases and equals D = 2.5 μm. For the PLGA layer, the values for r_V and D_{equiv} were as in Ref. [17]. The drug release curves show a delay of the drug passage through the math, which is a desirable effect in the implant design.

4. A summary and concluding remarks

We have briefly summarized the main characteristics of the KTM model. The generality and robustness of this methodology are illustrated by comparison with other typical approaches available in the literature. The goal of this short study was to emphasize that this quite straightforward method also provides a basis for further additions of specificities in medicine, biology, and science to model various complex multiscale and multiphysics problems. For example, it is suggested to include in the KTM the kinetics of the ligand-receptor binding as a straightforward generalization. We have illustrated the KTM generality by a selection of a few characteristic examples from our earlier publications. The first example demonstrates the determination of the effective partitioning coefficients in drug release from nanoparticles. These coefficients are further implemented in our connectivity elements within the KTM as a unique feature in modeling biological barriers. The next example serves to show the applicability of the KTM to large-scale models, with a multiscale description. The FE model of the entire pancreas is generated from images and it includes large vessels, extracellular space, capillary and lymphatic systems; and two groups of cells with their organelles and hydrophobic properties of transported molecules. Further, the multiphysics character of the KTM is shown in an example where the electrical field and diffusive transport of ions are coupled. Furthermore, this example demonstrates how general and complex phenomena in transport through biological barriers (here coupled cell membrane electrical potential and diffusion) can be included in the KTM. Finally, a simple example from our recent study of lung modeling is presented where the mechanics of lung deformation (with its microstructural deformation) is coupled to multiscale

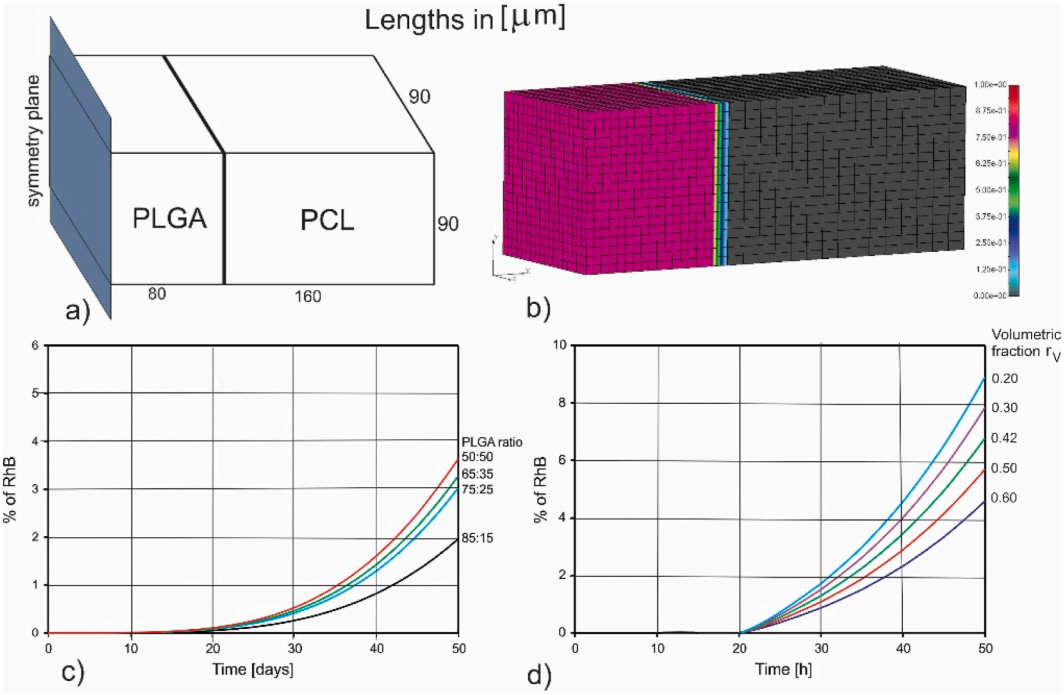

Fig. 17. Three-layered PCL/PLGA/PCL scaffold. a) Geometry of the model, b) Concentration field within the fibers (fiber domain of the KTM) at t = 50 days; c) Cumulative drug release (in percent) vs. time for the RhB impregnated into standard PLGA complexes with the LA/GA ratio: 50:50, 65:35, 75:25, and 85:15; d) Drug release vs. time for RhB complex impregnated into 24 wt% 65:35 PLGA, for several volume fractions of fibers within the PCL layer.

particulate transport within the lung airway generations. Additional two examples are given in support of the KTM generality – drug transport through a growing tumor (the KTM model generated from images), and a drug release from nanofibers with fiber degradation.

From the presented short analysis and illustrative examples that outline the concept and uniqueness of the KTM, it can be concluded that the KTM, due to its generality, ease and straightforward application, and efficiency, can serve as a tool in the development of today's important expert systems for everyday medical practice.

5. Data availability statement

The data that has been used is confidential.

Funding statement

This research was funded by the National Institute of Health (grant U01CA244107), as well as the Ministry of Education, Science and Technological Development of the Republic of Serbia, contract numbers 451-03-68/2023-14/200107 (Faculty of Engineering, University of Kragujevac), 451-03-66/2024-03/200378 (Institute for Information Technologies Kragujevac, University of Kragujevac); grant number F-134 (Serbian Academy of Sciences and Arts). The research was partially funded by the Golfers Against Cancer (C.S.F.) and funds from Houston Methodist Research Institute (C.S.F.). The authors are thankful to the City of Kragujevac, Serbia.

CRediT authorship contribution statement

Milos Kojic: Writing – original draft, Methodology, Conceptualization. **Miljan Milosevic:** Writing – review & editing, Software, Methodology. **Vladimir Simic:** Writing – review & editing, Visualization, Validation, Software. **Bogdan Milicevic:** Writing – review & editing, Visualization, Validation, Software. **Rossana Terracciano:** Writing – review & editing, Validation, Investigation, Data curation. **Carly S. Filgueira:** Writing – review & editing, Validation, Investigation, Data curation.

Declaration of competing interest

The authors declare that they have no known competing financial interests or personal relationships that could have appeared to influence the work reported in this paper.

References

[1] Milos Kojic, Miljan Milosevic, Arturas Ziemys, Computational Models in Biomedical Engineering - Finite Element Models Based on Smeared Physical Fields: Theory, Solutions, and Software, Elsevier, 2022.

[2] T.S. Koh, L.H. Cheong, Z. Hou, Y.C. Soh, A physiologic model of capillary–tissue exchange for dynamic contrast-enhanced imaging of tumor microcirculation, IEEE Trans. Biomed. Engrg. 50 (2) (2003) 159–167.

[3] Eoin R. Hyde, Andrew N. Cookson, Jack Lee, Christian Michler, Ayush Goyal, Sochi Taha, Radomir Chabiniok, Matthew Sinclair, David A. Nordsletten, Jos Spaan, P. Jeroen, H.M. van den Wijngaard, Maria Siebes, Nicolas P. Smith, Multi-scale Parameterisation of a Myocardial perfusion model using Whole-Organ arterial networks, Ann. Biomed. Eng. (2013), https://doi.org/10.1007/s10439-013-0951-y.

[4] Eoin R. Hyde, Christian Michler, Jack Lee, Andrew N. Cookson, Radek Chabiniok, David A. Nordsletten, Nicolas P. Smith, Parameterisation of multi-scale continuum perfusion models from discrete vascular netwok, Med. Biol. Eng. Comput. 51 (2013) 557–570.

[5] S. Di Gregorio, M. Fedele, G. Pontone, A.F. Corno, P. Zunino, C. Vergara, A. Quarteroni, A Multiscale Computational Model of Myocardial Perfusion in the Human Heart, MOX, Dipartimento di Matematica Politecnico di Milano, 2019.

[6] A. Corrias, P. Pathmanathan, D.J. Gavaghan, M.L. Buista, Modelling tissue electrophysiology with multiple cell types: applications of the extended bidomain framework, Integr. Biol. 4 (2012) 192–201.

[7] Milos Kojic, Smeared concept as a general methodology in finite element modeling of physical fields and mechanical problems in composite media, J. Serb. Soc. Comp. Mech. 12 (No.2) (2018) 1–16.

[8] M. Kojic, M. Milosevic, V. Simic, E.J. Koay, J.B. Fleming, S. Nizzero, N. Kojic, A. Ziemys, M. Ferrari, A composite smeared finite element for mass transport in capillary systems and biological tissue, Comp. Meth. Appl. Mech. Engrg. 324 (2017) 413–437, https://doi.org/10.1016/j.cma.2017.06.019.

[9] M. Kojic, M. Milosevic, V. Simic, E.J. Koay, N. Kojic, A. Ziemys, M. Ferrari, Extension of the composite smeared finite element (CSFE) to include lymphatic system in modeling mass transport in capillary systems and biological tissue, J. Serb. Soc. Comp. Mech. 11 (No.2) (2017) 108–120.

[10] Milos Kojic, Vladimir Simic, Miljan Milosevic, Composite smeared finite element – some aspects of the formulation and accuracy, | ISSN 1820 – 4511, IPSI Transactions on Advanced Research 13 (2) (2017). July2017.

[11] M. Kojic, M. Milosevic, V. Simic, D. Stojanovic, P. Uskokovic, A radial 1D finite element for drug release from drug Loaded nanofibers, J. Serb. Soc. Comp. Mech. 11 (1) (2017) 82–93.

[12] M. Kojic, M. Milosevic, N. Kojic, E.J. Koay, J.B. Fleming, [M. Ferrari, A. Ziemys, Mass release curves as the constitutive curves for modeling diffusive transport within biological tissue, Comput. Biol. Med. 92 (2018) 156–167, https://doi.org/10.1016/j.compbiomed.2016.06.026, 2016.

[13] M. Kojic, M. Milosevic, V. Simic, E.J. Koay, N. Kojic, A. Ziemys, M. Ferrari, Multiscale smeared finite element model for mass transport in biological tissue: from blood vessels to cells and cellular organelles, Comput. Biol. Med. 99 (2018) 7–23, https://doi.org/10.1016/j.compbiomed.2018.05.022.

[14] M. Kojic, M. Milosevic, V. Simic, A. Ziemys, N. Filipovic, M. Ferrari, Smeared multiscale finite element model for electrophysiology and ionic transport in biological tissue, Comput. Biol. Med. 108 (2019) 288–304.

[15] M. Milosevic, V. Simic, B. Milicevic, E.J. Koay, M. Ferrari, A. Ziemys, M. Kojic, Correction function for accuracy improvement of the Composite Smeared Finite Element for diffusive transport in biological tissue systems, Comp. Meth. Appl. Mech. Engrg. (2018), https://doi.org/10.1016/j.cma.2018.04.012.

[16] Miljan Milosevic, Dusica Stojanovic, Vladimir Simic, Bogdan Milicevic, Andjela Radisavljevic, Petar Uskokovic, Milos Kojic, A computational model for drug release from PLGA implant, Materials 11 (12) (2018) 2416, https://doi.org/10.3390/ma11122416, 2018.

[17] M. Milosevic, D.B. Stojanovic, V. Simic, M. Grkovic, M. Bjelovic, P.S. Uskokovic, M. Kojic, Preparation and modeling of three-layered PCL/PLGA/PCL fibrous scaffolds for prolonged drug release, Sci. Rep. 10 (1) (2020 Jul 7) 11126, https://doi.org/10.1038/s41598-020-68117-9. Erratum in: Sci Rep. 2021 Aug2;11(1): 16028, 2021.

[18] M. Kojic, N. Filipovic, M. Milosevic, Pak-Bio, Finite Element Program for Bioengineering Problems, Bioengineering R&D Center, and University of Kragujevac, Serbia, 2020.

[19] Altug Ozcelikkale, Hye-ran Moon, Michael Linnes and Bumsoo Han, *In vitro* microfluidic models of tumor microenvironment to screen transport of drugs and nanoparticles, WIREs Nanomed Nanobiotechnol (2017) e1460, https://doi.org/10.1002/wnan.1460.

[20] Chong T. Ying, Juntian Wang, Robert J. Lamm, Daniel T. Kamei, Mathematical modeling of vesicle drug delivery systems 2: Targeted vesicle interactions with cells, tumors, and the Body, J. Lab. Autom. 18 (1) (2013) 46–62.

[21] M. Kojic, Multiscale composite 3d finite element for lung mechanics, J. Serbian Soc. Comp. Mech. 14 (1) (2020) 1–11.

[22] M. Kojic, M. Milosevic, Blanco E. Wu, M. Ferrari, A. Ziemys, Mass partitioning effects in diffusion transport, Phys. Chem. Chem. Phys. 17 (2015) 20630–20635.

[23] M. Kojic, A multiscale multiphysics finite element for lung, J. Serbian Soc. Comp. Mech (2023) submitted for publication.

[24] R. Terracciano, B. Milićević, M. Milošević, V. Simić, Y. Carcamo-Bahena, A.L.R. Royal, A.A. Carcamo-Bahena, E.B. Butler, A. Grattoni, M. Kojić, C.S. Filgueira, An Insight into Perfusion Anisotropy within Solid Murine Lung Cancer Tumors, 2023 in preparation.

[25] J.F. Mano, R.A. Sousa, L.F. Boesel, N.M. Neves, R.L. Reis, Bioinert, biodegradable and injectable polymeric matrix composites for hard tissue replacement: State of the art and recent developments, Compos. Sci. Technol. 64 (2004) 789–817.

[26] H.R. Lin, C.J. Kuo, C.Y. Yang, S.Y. Shaw, Y.J. Wu, Preparation of macroporous biodegradable PLGA scaffolds for cell attachment with the use of mixed salts as porogen additives, J. Biomed. Mater. Res. 63 (2002) 271–279.

[27] L. Lu, S.J. Peter, M.D. Lyman, H. Lai, S.M. Leite, J.A. Tamada, S. Uyama, J.P. Vacanti, R. Langer, A.G. Mikos, In vitro and in vivo degradation of porous poly (-lactic-co-glycolic acid) foams, Biomaterials 21 (2000) 1837–1845.

[28] T.G. Park, Degradation of poly (lactic- co-glycolic acid) microspheres: effect of copolymer composition, Biomaterials 16 (1995) 1123–1130.

[29] H.K. Makadia, S.J. Siegel, Poly lactic-co-glycolic acid (PLGA) as biodegradable Controlled drug delivery Carrier, Polymers 3 (3) (2011) 1377–1397, https://doi.org/10.3390/polym3031377.

[30] A. Ziemys, M. Kojic, M. Milosevic, N. Kojic, F. Hussain, M. Ferrari, A. Grattoni, Hierarchical modeling of diffusive transport through nanochannels by coupling molecular dynamics with finite element method, J. Comput. Phys. 230 (2011) 5722–5731, https://doi.org/10.1016/j.jcp.2011.03.054.